Soil Response to Repetitive Changes in Pore-Water Pressure under Deviatoric Loading

Junghee Park[1] and J. Carlos Santamarina, A.M.ASCE[2]

Abstract: Soils often experience repetitive changes in pore water pressure. This study explores the volumetric and shear response of contractive and dilative sand specimens subjected to repetitive changes in pore water pressure, under constant deviatoric stress in a triaxial cell. The evolution towards a terminal void ratio e_T characterizes the *volumetric response*. The terminal void ratio e_T for pressure cycles falls below the critical state line, between $e_{\min} < e_T < e_{cs}$. Very dense specimens only dilate if they reach high stress obliquity $\eta_{\max}$ during pressurization. The terminal void ratios for very dense and medium dense specimens do not converge to a single trend. The *shear deformation* may stabilize at shakedown, or continue in ratcheting mode. The maximum stress obliquity $\eta_{\max}$ is the best predictor of the asymptotic state; shakedown prevails in all specimens subjected to stress obliquity $\eta_{\max} < 0.95 \cdot \eta_{cs}$ and ratcheting takes place when the maximum stress obliquity approaches or exceeds $\eta_{\max} \geq 0.95 \cdot \eta_{cs}$. Volumetric and shear strains can accumulate when the strain level during pressure cycles exceeds the volumetric threshold strain (about 5×10^{-4} in this study). A particle-level analysis of contact loss and published experimental data show that the threshold strain increases with confinement p'_o. **DOI: 10.1061/(ASCE)GT.1943-5606.0002229.** *This work is made available under the terms of the Creative Commons Attribution 4.0 International license, http://creativecommons.org/licenses/by/4.0/.*

Author keywords: Ratcheting; Pore water pressure cycle; Shakedown; Stress obliquity; Terminal void ratio.

Introduction

Soils experience repetitive changes in pore water pressure during groundwater level oscillations associated with tidal and river level fluctuations, and engineered structures such as docks and managed reservoirs (O'Reilly and Brown 1991; Chu et al. 2003; Orense et al. 2004; Leroueil et al. 2009; Page et al. 2010; Nakata et al. 2013; Shi et al. 2016). Coupled processes may also cause pore-fluid pressure oscillations, for example, in the case of a soft clay subjected to temperature cycles (Abuel-Naga et al. 2007).

Pore-fluid pressure fluctuations affect a wide range of geotechnical systems from foundations and slope stability to pumped-storage hydroelectric power stations, aquifer storage and recovery systems, compressed air energy storage, enhanced oil recovery by cyclic water flooding and cyclic steam injection, and repetitive CO_2 injection (Premchitt et al. 1986; Olson et al. 2000; Gambolati and Teatini 2015; Huang 2016; Chang et al. 2017).

Soils gradually deform in response to all kinds of repetitive excitations. Repetitive changes in water pressure imply effective stress cycles that can lead to the accumulation of plastic volumetric and shear strains. This study explores the volumetric and shear response of contractive and dilative sands subjected to repetitive changes in pore water pressure under constant deviatoric stress. The following section presents a detailed review of the state of the art and identifies salient gaps in knowledge.

[1]Postdoctoral Fellow, Earth Science and Engineering, King Abdullah Univ. of Science and Technology, Thuwal 23955-6900, Saudi Arabia (corresponding author). ORCID: https://orcid.org/0000-0001-7033-4653. Email: junghee.park@kaust.edu.sa

[2]Professor, Earth Science and Engineering, King Abdullah Univ. of Science and Technology, Thuwal 23955-6900, Saudi Arabia.

Note. This manuscript was submitted on July 8, 2018; approved on October 30, 2019; published online on March 10, 2020. Discussion period open until August 10, 2020; separate discussions must be submitted for individual papers. This paper is part of the ***Journal of Geotechnical and Geoenvironmental Engineering***, © ASCE, ISSN 1090-0241.

Previous Studies: Asymptotic States

Pore-Fluid Pressure Oscillation

Previous studies explored the effects of repetitive changes in pore-fluid pressure in the context of engineering needs, such as slope failures (Nakata et al. 2013) or aquifer oscillations (Hung et al. 2012). The selected test boundary conditions reflected field situations: triaxial stress (clays, Ohtsuka and Miyata 2001; Ohtsuka 2007), plane strain conditions (sand, Nakata et al. 2013), and K_o-conditions (sand-silt mixtures, Chang et al. 2017). In all cases, the strain accumulation induced by repetitive changes in pore-fluid pressure became more significant with an increasing pressure amplitude Δu_w. However, previous studies did not separate the volumetric response from the shear response; these are analyzed next.

Volumetric Asymptotic State: Terminal Void Ratio

All soils evolve towards an asymptotic terminal void ratio during repetitive loading (Narsilio and Santamarina 2008—Refer to the p'-e quadrant in Fig. 1). The tendency towards a terminal state is apparent in published data for all types of repetitive loads: pore-water pressure cycles (Chang et al. 2017), K_o-loading and deviatoric stress cycles (Triantafyllidis et al. 2004; Wichtmann et al. 2005; Chong and Santamarina 2016), freeze-thaw (Viklander 1998), dry-wet (Albrecht and Benson 2001), and chemical cycles (Musso et al. 2003). There are irreversible structural changes during repetitive loading and soil properties adapt as the soil transitions towards the terminal void ratio; for example, the fabric changes of clays during dry-wet cycles (Croney and Coleman 1954), permeability increases in freeze-thaw cycles and dry-wet cycles (Chamberlain et al. 1990; Albrecht and Benson 2001), shear strength increases in freeze-thaw cycles (Ono and Mitachi 1997; Qi et al. 2006), and there is gradual stiffening in cyclic K_o loading (Park and Santamarina 2019).

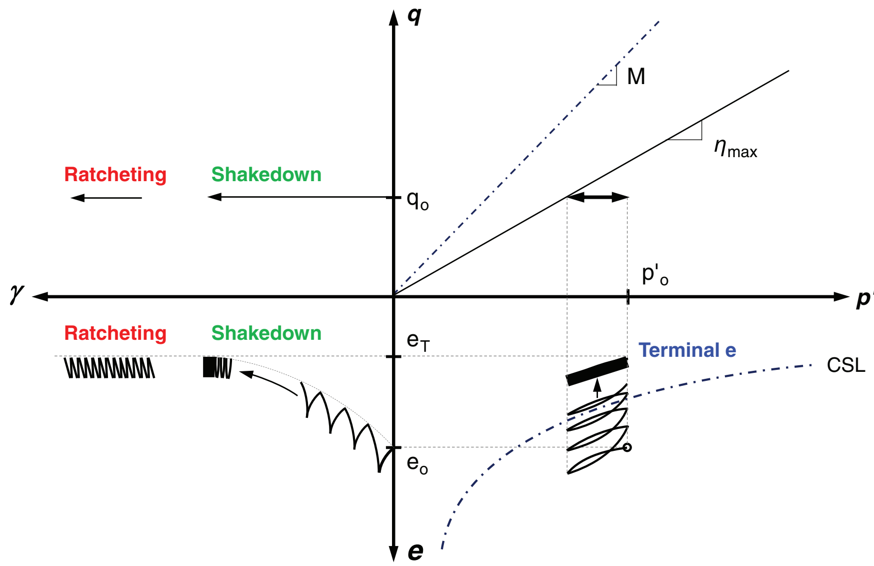

Fig. 1. (Color) Anticipated soil response to pore water pressure cycles under constant deviatoric loading. The plot captures asymptotic conditions in shear strain (shakedown or ratcheting) and volumetric strain (terminal void ratio e_T).

Shear Asymptotic State: Shakedown or Ratcheting?

The asymptotic condition in shear governs the response of all structures, from pavements (Sharp and Booker 1984) to metals (Johnson 1986). The shear response falls into one of three asymptotic regimes, as observed on the q-γ quadrant in Fig. 1 (Alonso-Marroquin and Herrmann 2004; Werkmeister et al. 2005)

- *Elastic shakedown*: non-hysteretic, fully recoverable deformation in every cycle.
- *Plastic shakedown*: hysteretic stress-strain response without permanent deformation at the end of each cycle.
- *Ratcheting*: the stress strain response is hysteretic, and there is continued plastic strain accumulation in every cycle.

The asymptotic condition depends on the stress amplitude ratio, the cyclic stress ratio $\Delta\sigma_z^{amp}/2p_o'$, and the cyclic shear stress level $\Delta\tau_{z\theta}^{amp}/\Delta\sigma_z^{amp}$ (Wu et al. 2017; Cai et al. 2018; Gu et al. 2018). Ratcheting should be expected at large stress amplitudes and high stress obliquity $\eta = q/p'$. It may also develop when a large number of cycles reaches a fatigue-induced tipping point, or when the stress level causes particle crushing (see data in Werkmeister 2003; Alonso-Marroquin and Herrmann 2004; Werkmeister et al. 2005; Wichtmann et al. 2005; da Fonseca et al. 2013).

Experimental Study

Tested Sand: Properties

Table 1 summarizes the main characteristics of the "KAUST 20/30 sand" used throughout this study and includes index properties such as the particle shape, the coefficient of uniformity C_u, and the extreme void ratios $e_{\max}$ and $e_{\min}$. Measured values are compared against predicted values from index properties for self-consistent verification (refer to Table 1 for details).

The critical state provides a "reference asymptotic state" for this study. Fig. 2 shows data for a set of conventional consolidated-undrained CU triaxial tests projected onto p'-q-ε_z-e-u planes.

Table 1. Tested sand—Properties

Property	KAUST 20/30 sand	Observations (Verifications using index test data)
Particle diameter	$d = 0.60 \sim 0.85$	
Roundness	$R = 0.60$	Image analysis—Roundness $R = \sum r_i/N$. The average radius of curvature of surface features divided by the radius of the largest inscribed sphere $r_{\max}$
Coefficient of uniformity	$C_u = 1.20$	
Specific gravity	$G_s = 2.65$	
Maximum void ratio	$e_{\max} = 0.786$	Estimated maximum void ratio: $e_{\max} = 0.76$ (Youd 1973)
Minimum void ratio	$e_{\min} = 0.533$	Estimated minimum void ratio: $e_{\min} = 0.54$ (Cho et al. 2006)
Friction angle at constant volume shear	$\phi_{cs} = 31°$	Angle of repose method: $\phi_{cs} = 32°$ (Santamarina and Cho 2001) Inferred from roundness is $\phi_{cs} = 31° \pm 2°$ (Cho et al. 2006)
Critical state line	$\Gamma = 0.845$	Intercept of *CSL* at 1 kPa
CSL in e-log p'	$\lambda = 0.074$	Slope of *CSL*
Shear wave velocity parameters	$\alpha = 89$ m/s $\beta = 0.21$	Corresponds to Hertzian-based power model $V_s = \alpha \cdot [p_o'/\text{kPa}]^\beta$ Note: α and β values for $e_o = 0.65$
Estimated threshold strain for contact loss in monotonic loading	$\gamma_{th}\vert^{loss} = 5 \times 10^{-4}$	Based on contact-loss analysis: $\gamma_{th}\vert^{loss} = 1.3 \cdot (\sigma_o'/G_g)^{2/3}$ Confining stress $\sigma' = 250$ kPa Mineral: $G_g = 30$ GPa and $\upsilon = 0.25$ (assumed in analysis)

Note: Measured values are compared against values predicted from index properties for self-consistent verification.

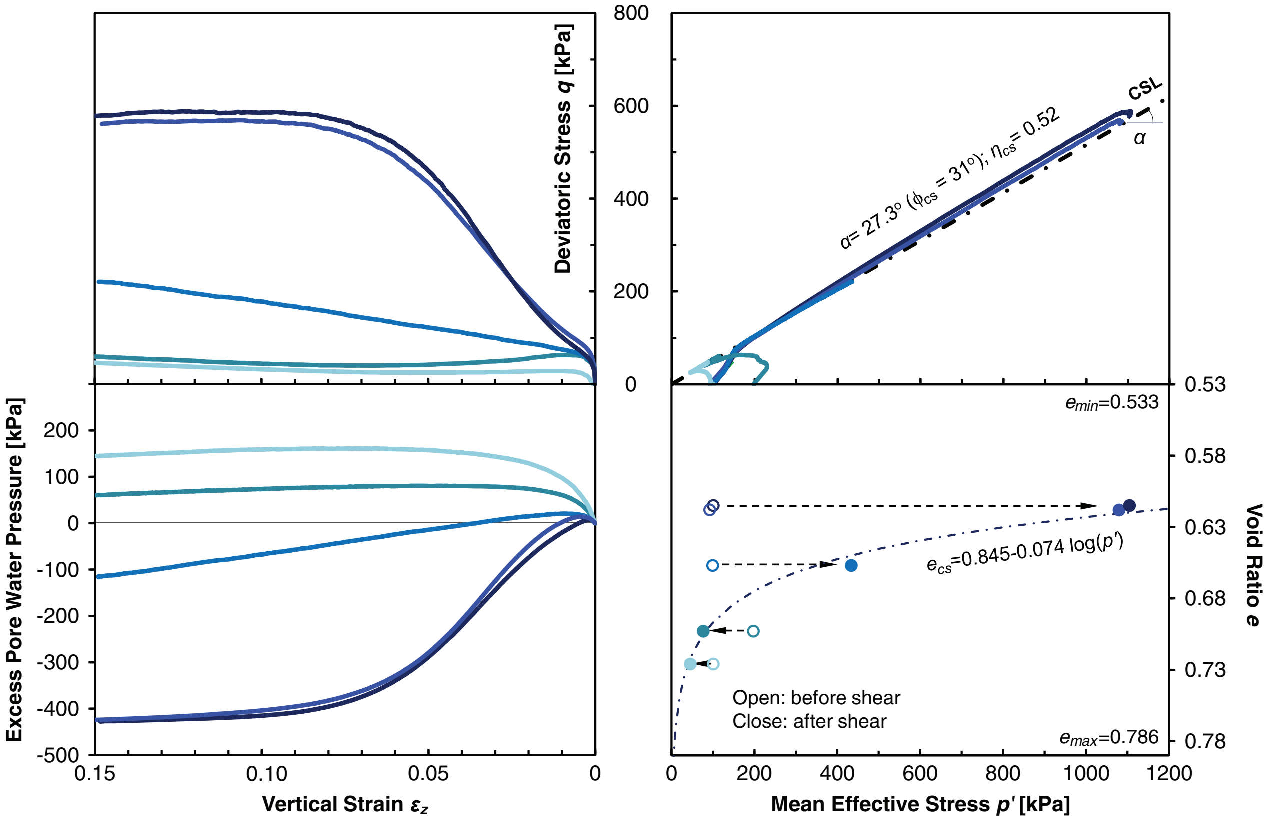

Fig. 2. (Color) Conventional consolidated, undrained CU triaxial test data projected onto u_w-ε_z-q-p'-e planes (strain rate: $\varepsilon_z = 0.01/\text{min}$). Notation: $p' = (\sigma_1' + \sigma_3')/2$, $q = (\sigma_1' + \sigma_3')/2$, $\phi_{cs} = \sin^{-1}(\tan\alpha)$, and stress obliquity $\eta = q/p'$. Critical state parameters for the KAUST 20/30 sand: friction angle $\phi_{cs} = 31^\circ$, intercept of CSL at 1 kPa in e-log $p' = 0.845$, and slope of CSL in e-log $p' = 0.074$. For reference, the maximum and minimum void ratios are $e_{\max} = 0.786$ and $e_{\min} = 0.533$.

Table 1 lists the critical state parameters obtained for the KAUST 20/30 sand. Measured values are consistent with values estimated from index properties (Refer to Table 1 for details).

Experimental Devices and Configuration

The triaxial system used to conduct the repetitive pressure cycles consists of (1) a triaxial cell with an LVDT (Linear Variable Differential Transformer) to track the vertical displacement, (2) a loading frame to apply a constant deviatoric stress, and (3) a pressure panel that generates cyclic changes in pore water pressure and measures volume changes.

Sample Preparation

We prepare loose, medium dense, and dense specimens using a combination of raining and tamping techniques to obtain different initial relative densities between $D_r = 15\%$ and 70%.

Loading Histories

We can simulate the effects of changes in water pressure through changes in either the back pressure or the confining pressure (Brenner et al. 1985; Anderson and Sitar 1995; Farooq et al. 2004; Orense et al. 2004). The two test procedures yield the same results if the Biot's coefficient $\chi = 1 - B_{sk}/B_g$ remains close to $\chi \approx 1.0$, that is at a relatively low confining effective stress (note: B_{sk} is the bulk modulus of the soil skeleton, and B_g is the bulk modulus of the mineral that makes the grains, Skempton 1961; Santamarina et al. 2001). In this study, we control the back pressure u_w.

Fig. 3 presents a subset of the stress paths explored in this study. Typical loading histories consist of five stages (1) isotropic consolidation, (2) drained deviatoric loading to stress obliquity $\eta = 0.33$, (3) a decrease in back pressure u_w to reach $\eta = 0.20$, (4) repetitive changes in pore water pressure from $\eta = 0.20$ to $\eta_{\max} = 0.50$ for $N = 100$ loading cycles (shown in red), and (5) strain-controlled undrained axial compression from $\eta = 0.20$ to failure at a vertical strain rate of $\varepsilon_z = 0.01/\text{min}$. Table 2 summarizes the experimental study. Test parameters include the initial void ratio e_o, cyclic pressure amplitude Δu_w, and maximum stress obliquity $\eta_{\max} = q/p'_{\min}$. Cyclic pressure amplitudes Δu_w selected for this study represent various field conditions, such as tidal action (<170 kPa at Burntcoat Head and Leaf Basin in North America), seasonal fluctuations in ground water levels (70–100 kPa,—Hung et al. 2012; Huang 2016), injection pressures for injection wells and injection-recovery wells used in aquifer storage (<500 kPa,—Shi et al. 2016; Page et al. 2010), and some coupled processes (e.g., geothermally-induced Δu_w < 250 kPa,—Laloui 2001; Abuel-Naga et al. 2007).

Experimental Results

This section reports detailed experimental results for two sets of tests designed to explore the effects of maximum stress obliquity $\eta_{\max}$ and initial confinement p'_o. We analyze the complete dataset gathered in this study in the following section.

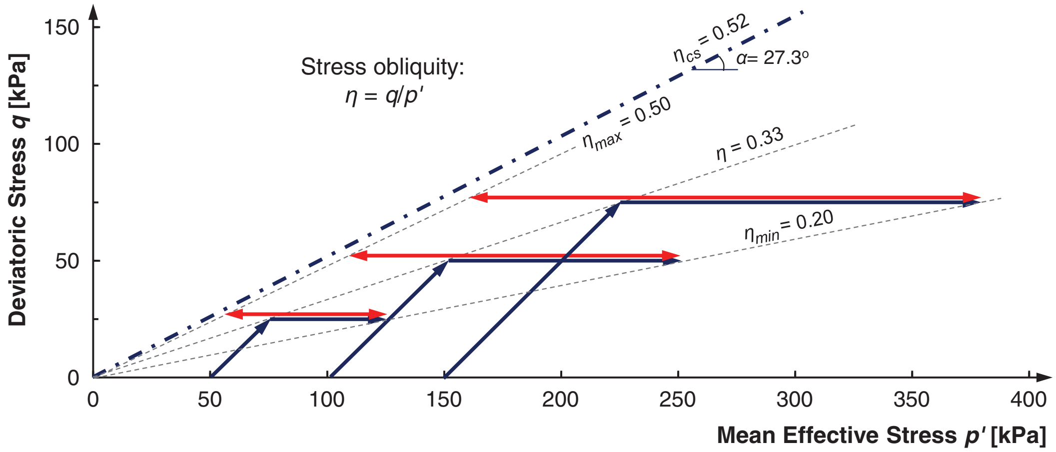

Fig. 3. (Color) Stress paths on the p'-q space (a subset of cases is shown here. Refer to Table 1 for a complete description). The loading history consists of five stages: (1) isotropic consolidation, (2) drained deviatoric loading to stress obliquity $\eta = 0.33$, (3) decrease back pressure u_w to reach $\eta = 0.20$, (4) repetitive change in pore water pressure from $\eta = 0.20$ to $\eta_{\max} = 0.50$ (shown in red), and (5) strain-controlled undrained axial compression from $\eta = 0.20$ to failure at a strain rate of $\varepsilon_z = 0.01/\text{min}$. Notation: $p' = (\sigma_1{}' + \sigma_3{}')/2$, $q = (\sigma_1{}' + \sigma_3{}')/2$, $\phi_{cs} = \sin^{-1}(\tan\alpha)$.

Study 1: Maximum Stress Obliquity $\eta_{\max}$

Fig. 4 illustrates the load-deformation response of loose and medium dense sands initially loaded to the same $p' = 250$ kPa and $\eta_{\min} = 0.20$, and subjected to repetitive fluid pressure cycles to different maximum stress obliquities $\eta_{\max} = 0.33$, 0.40, 0.45, and 0.50 (Fig. 3). The results show

- *Pre-loading*. The void ratio decreases during isotropic confinement ($p' = 100$ kPa, $q = 0$) and deviatoric loading ($p' = 150$ kPa, $q = 50$ kPa). The vertical strain is very similar in all specimens as the stress obliquity reaches the initial value of $\eta_o = 0.33$ and during the first decrease in pore water pressure to reach $\eta_{\min} = 0.20$.
- *Repetitive pressure cycles*. All specimens exhibit volume dilation every time the pore pressure increases (the mean stress decreases, and obliquity increases from $\eta_{\min} \to \eta_{\max}$); however, there is residual contraction at the end of the cycle. The vertical strain increases during pressurization ($\eta_{\min} \to \eta_{\max}$) and accumulates at the end of every cycle. Volumetric contraction and vertical strain accumulation are more pronounced in specimens that reach a higher maximum stress obliquity $\eta_{\max}$ during pressure cycles. Note that the initial void ratio e_o of all specimens falls in the contractive zone just before repetitive loading; thereafter, the two specimens subjected to large pressure cycles ($\eta_{\max} = 0.50$ and $\eta_{\max} = 0.45$) become denser than at the critical state.
- *Undrained shear*. All specimens reach the critical state line during the undrained deviatoric loading that followed the $N = 100$ pressure cycles (p'-q-e space in Fig. 4). These results confirm that in the absence of overt localization the critical state line is not affected by the monotonic or cyclic loading history (Taylor 1948; Schofield and Wroth 1968; Castro et al. 1982; Mohamad and Dobry 1986).

Study 2: Confining Effective Stress p'

Fig. 5 shows the p'-q-e-ε_z load-deformation response of three medium dense specimens subjected to different initial mean stress values p'_o. Initial conditions include specimens above and below the critical state line. Details of the loading history before repetitive loading is shown in Fig. 3. Pressure cycles cause changes in obliquity from $\eta_{\min} = 0.20$ to $\eta_{\max} = 0.50$ in all cases. The changes in void ratio and the vertical strain accumulation during the repetitive pressure cycles are more significant in the one specimen subjected to high initial mean stress p'_o. Once again, all specimens shear and dilate as the pressure increases. However the overall void ratio trend is contractive at the end of every cycle. All three specimens land on the dilative side of the critical state at the end of cyclic loading and exhibit a dilative tendency during the final undrained shear.

Analysis of the Complete Dataset

This section analyzes the results of all tests conducted in this study (Table 2), with an emphasis on the shear strains and volume changes that occur during repetitive pressure cycles. Within triaxial boundary conditions, the shear strain $\gamma = (3\varepsilon_z - \varepsilon_{vol})/2$ combines the vertical strain ε_z and the volumetric strain ε_{vol}. System compliance and inadequate saturation bias both the measured peak-to-peak volumetric strain and the computed peak-to-peak shear strain. Therefore, figures and analyses in this section place emphasis on incremental and cumulative strains determined at the same pressure at the end of each cycle.

Shear Deformation

Fig. 6 presents the shear strain accumulation as a function of pressure cycles. The initial mean stress is the same for all specimens, $p'_o = 250$ kPa, but pressure cycles reach different maximum stress obliquities $\eta_{\max}$. The shear strain accumulation model below fits data trends in all tests (modified from Chong and Santamarina 2016)

$$\gamma_i = \gamma_1 + a(1 - i^{-b}) - c(1 - i^{-1}) + d(i - 1) \tag{1}$$

where a, b, c, and d are fitting parameters, and i is the number of loading cycles. The shakedown response corresponds to $d = 0$, while $d > 0$ implies ratcheting. Table 2 summarizes the fitted model parameters for all tests. Results indicate that

- The shear strain accumulation induced by pressure cycles is more pronounced in earlier cycles, in loose sands, in specimens that experience a higher maximum stress obliquity $\eta_{\max}$ (for tests with the same initial p'_o), and in specimens subjected to a higher initial mean stress p'_o (for tests that reach the same $\eta_{\max}$).
- Shakedown is unmistakable for specimens with small $\eta_{\max}$. In general, all specimens subjected to stress obliquity $\eta_{\max} \le 0.50$

Table 2. Experimental study: Test conditions

Specimen characteristics				Pressure cycles: Stress conditions				Pressure cycles: Void ratio e				Pressure cycles: Shear strain γ^a					CU—AC
Conditions before pressure cycles relative to critical state	Test No.	Void ratio after specimen preparation	B-value	q [kPa]	Δu_w [kPa]	p'_{max} [kPa]	η_{max}	e_o	e_T	m^b	N^{*b}	γ_1	a	b	c	d	Volume change tendency during final undrained shear
Contractive side	1	0.7461	0.972	50	100	250	0.33	0.7065	0.7000	1.0	49	3.01×10^{-4}	0.090	0.0150	0.0015	0	Contractive
	2	0.7390	0.981	50	110	250	0.36	0.7027	0.6960	0.95	43	8.74×10^{-5}	0.113	0.0205	0.0013	0	No CU-AC
	3	0.7419	0.976	50	125	250	0.40	0.7031	0.6878	1.0	22	2.11×10^{-3}	0.234	0.0250	0.0060	0	Contractive
	4	0.7208	0.977	50	140	250	0.45	0.6828	0.6621	0.85	19	4.70×10^{-3}	0.410	0.0240	0.0080	0	Dilative
	5	0.7092	0.976	50	150	250	0.50	0.6722	0.6448	0.88	19	7.70×10^{-3}	0.775	0.0230	0.0160	0	Dilative
	6	0.7180	0.981	75	225	375	0.50	0.6660	0.6361	0.79	13	7.92×10^{-3}	0.800	0.0220	0	0	Dilative
Dilative side	7	0.6958	0.984	25	75	125	0.50	0.6783	0.6598	1.0	26	2.90×10^{-3}	0.625	0.0220	0.016	0	Dilative
	8	0.6138	0.950	50	55	250	0.26	0.5900	0.5915	0.9	1	2.86×10^{-4}	0.003	0.0400	0.00003	0	No CU-AC
	9	0.6171	0.952	50	85	250	0.30	0.6021	0.6032	1.0	1	3.02×10^{-4}	0.002	0.0280	0	0	No CU-AC
	10	0.6151	0.951	50	125	250	0.40	0.6015	0.6030	0.9	1	4.45×10^{-4}	0.010	0.0150	0.0001	0	No CU-AC
	11	0.6196	0.966	50	140	250	0.45	0.6025	0.6029	1.0	1	2.57×10^{-3}	0.075	0.0200	0.0001	0	Dilative
	12	0.6145	0.977	50	153	250	0.52	0.6000	0.6008	1.0	1	3.06×10^{-3}	0.080	0.0200	0.0001	0	Dilative
	13	0.6133	0.965	50	155	250	0.53	0.5965	0.6052	1.0	7	2.03×10^{-3}	0.170	0.0150	0	0	No CU-AC
	14	0.6200	0.967	50	160	250	0.56	0.6032	0.6415	1.0	24	3.54×10^{-3}	0.200	0.0500	0	4×10^{-4}	No CU-AC

Note: Fitting parameters correspond to models introduced in the text. q = deviatoric stress; Δu_w = cyclic pressure amplitude; p'_{max} = maximum mean stress at the end of depressurization cycle; η_{max} = maximum stress obliquity $(= q/p'_{min})$; e_o = initial void ratio at $i = 0$; e_T = terminal void ratio at $i \to \infty$; m = model parameter; N^* = characteristic number; γ_1 = shear strain at the end of first cycle $i = 1$; a, b, and c = model parameters; and d = ratcheting parameter.

[a]Shear strain accumulation model: $\gamma_i = \gamma_1 + a(1 - i^{-b}) - c(1 - i^{-1}) + d(i - 1)$.

[b]Void ratio evolution model: $e_i = e_T + (e_o - e_T)[1 + (i/N^*)^m]^{-1}$.

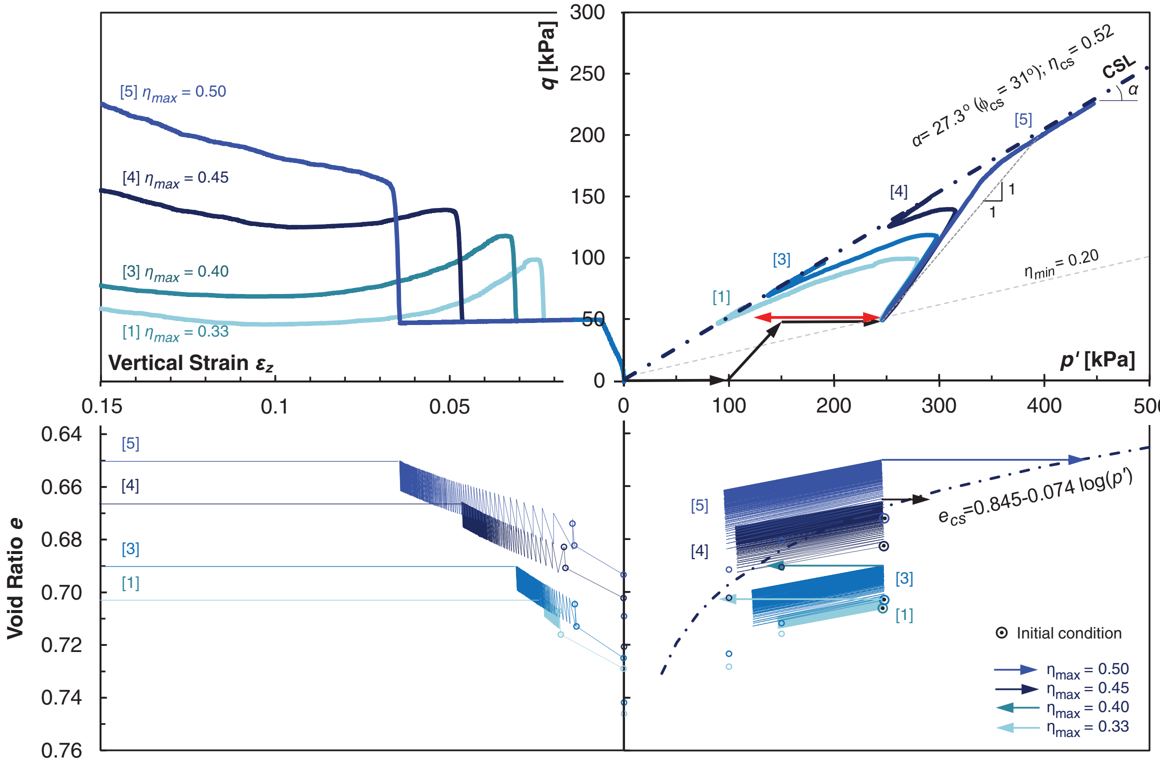

Fig. 4. (Color) Maximum stress obliquity: Loose and medium dense sands subjected to repetitive fluid pressure cycles to different maximum stress obliquities $\eta_{\max}$. In all four specimens, the pressure cycles begin at $p'_o = 250$ kPa and $\eta_{\min} = 0.20$. Tests end with undrained axial compression from the same initial stress condition at $\eta_{\min} = 0.20$. Notation: $p' = (\sigma_1' + \sigma_3')/2$, $q = (\sigma_1' - \sigma_3')/2$, $\phi_{cs} = \sin^{-1}(\tan\alpha)$, and stress obliquity $\eta = q/p'$. Numbers in square brackets [#] indicate the Test number in Table 2.

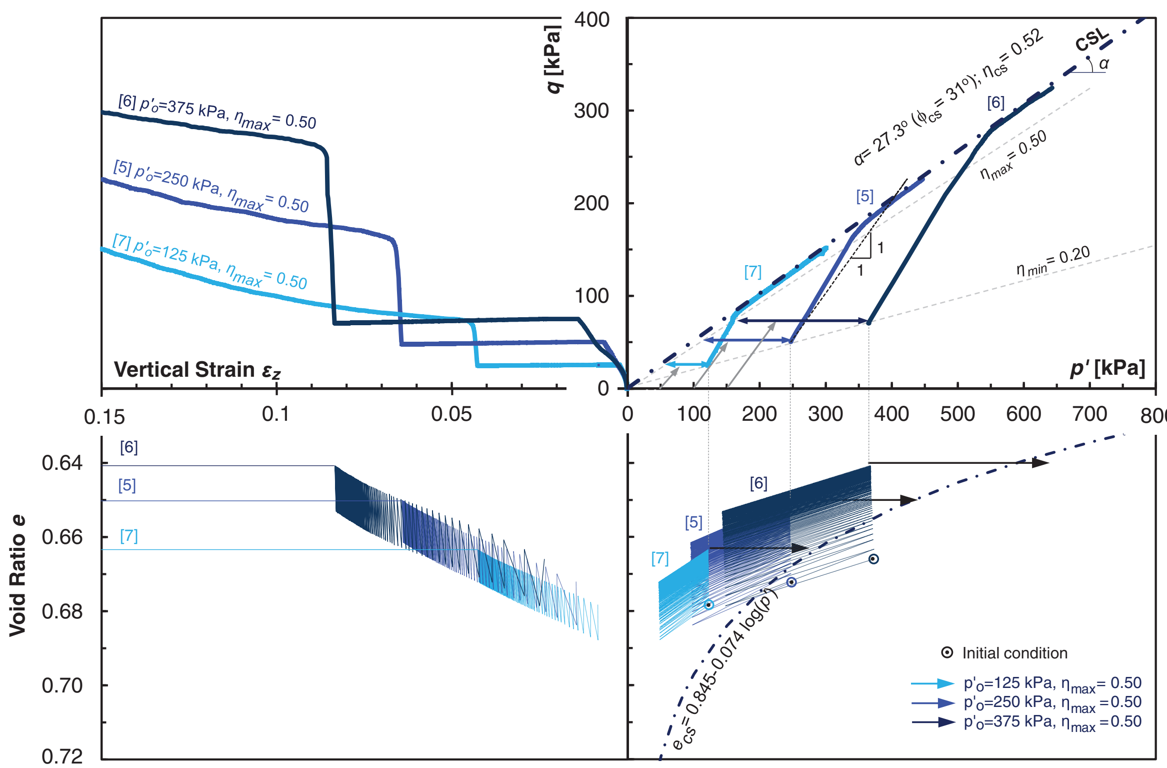

Fig. 5. (Color) Confining effective stress: Medium dense sand specimens subjected to repetitive fluid pressure cycles between $\eta_{\min} = 0.20$ and $\eta_{\max} = 0.50$. Tests end with undrained axial compression from the same obliquity $\eta_{\min} = 0.20$. Figure 2 shows all stress paths in detail. Notation: $p' = (\sigma_1' + \sigma_3')/2$, $q = (\sigma_1' - \sigma_3')/2$, $\phi_{cs} = \sin^{-1}(\tan\alpha)$, and stress obliquity $\eta = q/p'$. Numbers in square brackets [#] indicate the Test number in Table 2.

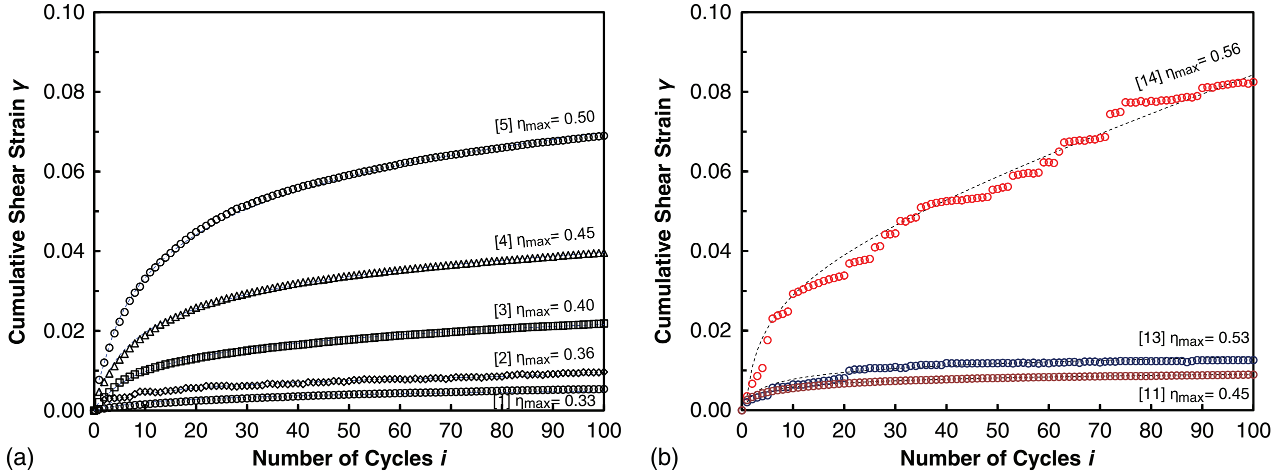

Fig. 6. (Color) *Shear deformation*: Cumulative shear strain γ versus number of cycles: (a) loose and medium dense specimens; and (b) dense specimens. The initial mean effective stress $p_o' = 250$ kPa and minimum stress obliquity is $\eta_{\min} = 0.20$ in all tests. The maximum stress obliquity $\eta_{\max}$ is indicated in each case. Dotted lines: Shear strain accumulation model fitted to test results [Eq. (1), Table 2 summarizes model parameters]. The obliquity at critical state is $\eta_{cs} = 0.52$. Numbers in square brackets [#] indicate the Test number in Table 2.

exhibit a shakedown response regardless of their initial density. For reference, the obliquity at critical state is $\eta_{cs} = 0.52$.

- The dense specimen subjected to pressure cycles above the critical state ($\eta_{\max} = 0.56$) shows a ratcheting response ($d = 4 \times 10^{-4}$). This specimen gradually dilates during pressure cycles. Hence the frictional resistance evolves from ϕ_{peak} towards ϕ_{cs}; eventually, a pressure cycle above critical state obliquity will cause the soil to fail.
- Overall, the initial packing density determines the different failure modes when soils are subjected to pressure fluctuations. Loose soil will contract. Dense soil will experience dilation when pressure cycles reach high stress obliquity (above values corresponding to ϕ_{cs}).

These observations indicate that shear strain accumulation is a function of the initial void ratio e_o, the initial confinement p_o', and the maximum stress obliquity $\eta_{\max}$ reached during pressure cycles.

Volume Change

Void Ratio

Fig. 7 presents the evolution of the void ratio with the number of cycles for all specimens where pressure cycles start at $p_o' = 250$ kPa. Specimens in Fig. 7 have distinct initial void ratios e_o (from $e_o = 0.59$ to $e_o = 0.71$; for reference, $e_{\min} = 0.533$ and $e_{\max} = 0.786$) and reach different maximum stress obliquity values $\eta_{\max}$. The highest rate of change in void ratio occurs during earlier pressure cycles and is more pronounced as the maximum stress obliquity increases. The void ratio e_i measured at the end of the i_{th} cycle evolves towards an asymptotic terminal void ratio e_T in all specimens. The following accumulation model properly fits all datasets (Park and Santamarina 2019):

$$e_i = e_T + (e_0 - e_T)\left[1 + \left(\frac{i}{N^*}\right)^m\right]^{-1} \quad \text{for } m > 0 \qquad (2)$$

where the m-exponent varies between $m = 0.8$ to 1.0. The model parameter N^* is the number of cycles required for a given specimen to reach half of the asymptotic volume change $(e_o - e_T)/2$. Table 2 lists fitted model parameters for all tests.

Discussion

Particle-Scale Deformation Mechanisms: Threshold Strain

In the absence of grain crushing, particle-scale deformation mechanisms relate to the strain level γ the soil experiences. There are two threshold strains under monotonic loading conditions

1. all deformations take place at contacts until the elastic threshold strain $\gamma \leq \gamma_{th}|^{el}$ that is selected at $G/G_{\max} \approx 0.99$, and
2. there are minimal fabric changes until the volumetric threshold strain $\gamma \leq \gamma_{th}|^{v}$. Typically, $\gamma_{th}|^{v} \approx 30 \cdot \gamma_{th}|^{el}$ (Sands: Vucetic 1994, Ishihara 1996. Clays: Díaz-Rodríguez and Santamarina 2001).

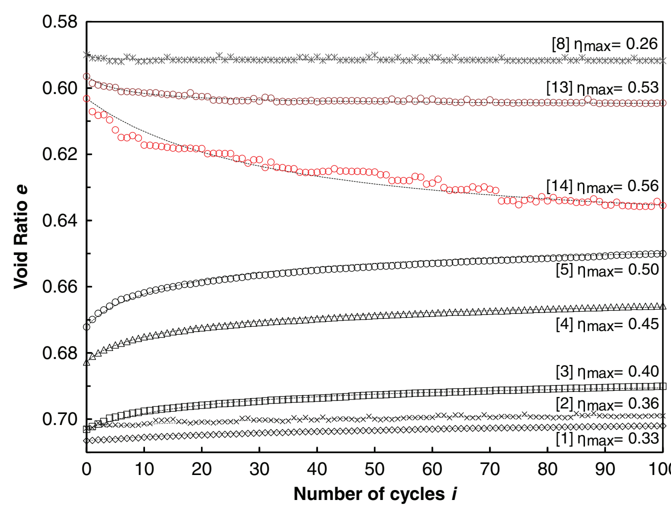

Fig. 7. (Color) *Volume change:* Void ratio versus number of cycles for loose, medium, and dense specimens subjected to fluid pressure oscillations. The initial mean effective stress $p_o' = 250$ kPa and minimum stress obliquity is $\eta_{\min} = 0.20$ is common to all tests. The maximum stress obliquity $\eta_{\max}$ is indicated in each case. Dotted lines: void ratio evolution model fitted to test results [Eq. (2), Table 2 summarizes model parameters]. The obliquity at critical state is $\eta_{cs} = 0.52$. Numbers in square brackets [#] indicate the Test number in Table 2.

J. Geotech. Geoenviron. Eng., 2020, 146(5): 04020023

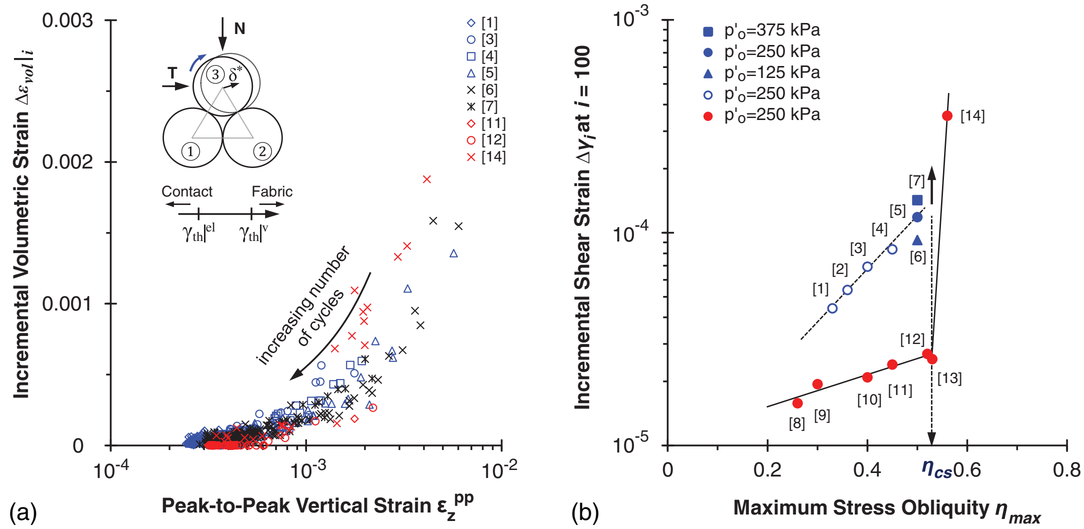

Fig. 8. (Color) Strain and obliquity thresholds: (a) incremental volumetric strain versus peak-to-peak vertical strain; and (b) incremental shear strain as a function of maximum stress obliquity at the $i = 100$ pressure cycle. Numbers in square brackets [#] indicate the Test number in Table 2.

Slip-down, grain roll-over, and high frictional losses take place at strains above the volumetric threshold (Ishihara 1996; Mueth et al. 2000).

Let's consider three spherical particles arranged in a triangular configuration and subjected to a normal force N [Fig. 8(a), inset]. The shear force T increases until the contact force F_{13} between particles ① and ③ becomes $F_{13} = 0$, which indicates contact loss. The extension of the 1 and 3 contact and the contraction of the 2 and 3 contact follow Hertzian behavior. Then, the horizontal displacement δ^* of the top particle ③ relative to the interlayer height $d \cdot \cos 30°$ yields the equivalent shear strain for contact loss $\gamma_{th}|^{loss}$ as a function of the mineral shear modulus G_g and the applied confining stress σ' estimated from the applied force as $\sigma' \propto N/d^2$ (Santamarina et al. 2001)

$$\gamma_{th}|^{loss} = 1.3\left(\frac{\sigma'}{G_g}\right)^{2/3} \tag{3}$$

This analysis anticipates that the threshold strain at contact loss increases with confining stress σ' in agreement with experimental evidence (Dyvik et al. 1984; Kim et al. 1991; Vucetic 1994). The threshold strain estimated using Eq. (3) is $\gamma_{th}|^{loss} \approx 5 \times 10^{-4}$ at $p'_o = 250$ kPa (Table 1; see data in Silver and Seed 1971; Dobry et al. 1982; Vucetic 1994; Santamarina and Shin 2009).

Clearly, there can be no volumetric strain accumulation when the cyclic strain level is too low for contact loss and fabric change. But, what is the threshold strain for repetitive pressure cycles? Let us compute the incremental volumetric strain in a given cycle $\Delta\varepsilon_{vol}|_i$ as a function of the change in void ratio between two consecutive cycles i and $i+1$ (taken at the same fluid pressure at the end of each cycle)

$$\Delta\varepsilon_{vol}|_i = \frac{e_i - e_{i+1}}{1 + e_i} \tag{4}$$

Fig. 8(a) shows the absolute value of the incremental volumetric strain $\Delta\varepsilon_{vol}|_i$ for contractive and dilative specimens plotted against the peak-to-peak vertical strain ε_z^{pp} for all cycles. Data trends show that (1) volumetric changes diminish as the number of pressure cycles increases, and (2) volumetric changes vanish $\Delta\varepsilon_{vol}|_i \to 0$ as the peak-to-peak vertical strain $\varepsilon_z^{pp} \to$ 2-to–5×10^{-4}.

Shakedown or Ratcheting?

The initial state of stress (p'_o, q_o) and void ratio e_o together with the amplitude of pressure cycles Δu_w and the maximum stress obliquity $\eta_{\max}$ determine the shear strain response of a soil subjected to repetitive changes in pore water pressure under constant deviatoric stress. The incremental shear strain $\Delta\gamma_i$ between two consecutive cycles i and $i+1$ scales with the maximum stress obliquity when $\eta_{\max} < 0.95 \cdot \eta_{cs}$, and gradually diminishes towards shakedown [Figs. 6(a) and 8(b)]. Ratcheting takes place when the maximum stress obliquity approaches or exceeds $\eta_{\max} \to \eta_{cs}$ [Figs. 6(b) and 8(b)]. Note that Wu et al. 2017 report the onset of ratcheting behavior at $\eta = 0.50$, i.e., close to failure.

Minimum Volumetric Strain

The volumetric strain $\varepsilon_{vol} = \Delta u/B_{\max}$ computed using the small-strain maximum skeletal bulk stiffness $B_{\max}$ provides a lower bound estimate of the volumetric strain the soil will experience during a given pressure cycle Δu_w. The maximum skeletal bulk stiffness can be computed from the in situ shear wave velocity $B_{\max} = 2 \cdot (V_s^2\rho)(1+\nu)/[3 \cdot (1-2\nu)]$, where ν is the small-strain Poisson's ratio. For example, consider a KAUST 20/30 specimen subjected to $p'_o = 250$ kPa and $\Delta u_w = 100$ kPa where the shear wave velocity for KAUST 20/30 sand increases with confining stress as $V_s = 89\ \text{m/s}(p'_o/1\ \text{kPa})^{0.21}$ and the small-strain Poisson's ratio is $\nu \approx 0.15$ (Note $e_o \approx 0.65$ in—Table 1). Then, the minimum peak-to-peak volumetric strain is $\varepsilon_{vol} \approx 6 \times 10^{-4}$.

Maximum Volumetric Strain

Terminal Void Ratio

Fig. 9(a) compares the initial void ratio e_o and the terminal void ratio e_T for specimens with different e_o, p'_o, and $\eta_{\max}$ (Note: $p'_o = 250$ kPa for the eight specimens in the dotted box, but symbols are p'-shifted to facilitate the visualization). Previous studies have suggested that there is a characteristic "terminal void ratio" for each loading condition (Narsilio and Santamarina 2008). Note that the critical state CS is the terminal state for monotonic shear. Results reported in this study show that loose to medium dense specimens contract to reach terminal void ratios that are denser than CS.

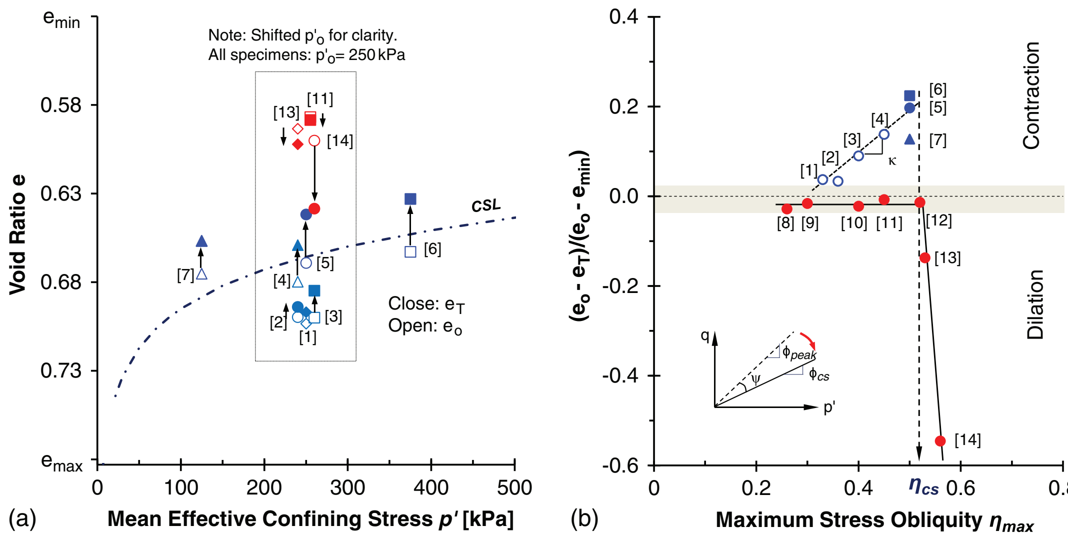

Fig. 9. (Color) Asymptotic volumetric response: (a) evolution of void ratio for medium dense (= blue) and dense sand (= red) specimens subjected to fluid pressure oscillations at different mean effective stress p_o'. Empty symbols show the initial void ratio e_o at the beginning of repetitive pressure cycles, while filled symbols show the terminal void ratio e_T. The repetitive changes in pore water pressure begin at $\eta_{\min} = 0.20$ in all specimens shown in this figure. The critical state line CSL is $e_{cs} = 0.845 - 0.074\ \log(p')$; and (b) normalized volume change $(e_o - e_T)/(e_o - e_{\min})$ caused by fluid pressure oscillations versus maximum stress obliquity $\eta_{\max}$—Loose, medium dense, and dense sand specimens. Numbers in square brackets [#] indicate the Test number in Table 2.

However, very dense specimens only dilate if pressurization causes high stress obliquity $\eta_{\max}$, and may rapidly evolve to failure without reaching a unique terminal state.

Potential Volume Change: Obliquity

Let us define the normalized asymptotic volume change $(e_o - e_T)/(e_o - e_{\min})$ in terms of the initial void ratio e_o at the beginning of pressure cycles ($i = 0$), the terminal void ratio e_T ($\to \infty$), and the minimum void ratio $e_{\min}$. Results discussed above suggest that the normalized volume change caused by fluid pressure cycles depends on the maximum stress obliquity $\eta_{\max}$ [Fig. 9(b)]. Contractive specimens experience volume change when obliquity exceeds $\eta_{\max} > 0.3$, and it is proportional to $\eta_{\max}$ thereafter. On the other hand, significant volumetric dilation in dense specimens requires a stress obliquity $\eta_{\max}$ greater than the critical state stress obliquity $\eta_{\max} \geq \eta_{cs} = 0.52$. The minimum void ratio $e_{\min}$, the void ratio at critical state e_{cs}, and the terminal void ratio for pressure cycles e_T are all "asymptotic states" for a given sand (where e_{cs} and e_T are initial stress dependent). The preceding results show that terminal void ratios fall below the critical state line between $e_{\min} < e_T < e_{cs}$. Together, Figs. 7–9 suggest that the balance between internal deformation mechanisms depends on initial stress conditions p_o' and q_o, the maximum obliquity $\eta_{\max}$ reached in pressure cycles and the initial void ratio e_o.

Design Guidelines

The volumetric strain ε_T associated with the maximum asymptotic change in void ratio $\Delta e = e_o - e_T$ induced by pressure cycles as $i \to \infty$ is

$$\varepsilon_T = \frac{e_0 - e_T}{1 + e_0} \tag{5}$$

We cannot propose a definitive approach to estimate the terminal volumetric strain ε_T for pressure cycles due to the limited dataset available at this time. However, the results in Fig. 9(b) suggest

- The terminal change in void ratio for loose and medium dense sands is a μ-fraction of the void ratio difference $e_o - e_{\min}$. In other words, $\Delta e_T = e_o - e_T = \mu \cdot (e_o - e_{\min})$.
- The μ-fraction is relatively low (i.e., $\mu \leq 0.3$) and is a function of the maximum stress obliquity $\eta_{\max}$.

Comparison between Pressure Cycles versus K_o-Loading Cycles

The terminal void ratio evolves to its asymptotic state when the sand is subjected to repetitive vertical loading under zero lateral strain (previously reported in Park and Santamarina 2019). While boundary conditions are very different, both studies show that

- There is a minimum strain required for plastic strain accumulation. The vertical threshold strain in the K_o cell varies in the range of 2 to 7×10^{-4}, which is similar to estimated values in this study.
- All specimens contract in K_o-loading cycles, but not in the pore-water pressure cycles with deviatoric loads (Fig. 7). Yet, the terminal void ratio falls between $e_o > e_T > (0.7 \cdot e_o + 0.3 \cdot e_{\min})$ in both K_o-loading and pressure cycle studies.

Ratio between Horizontal-to-Vertical Plastic Strains

The shear strain accumulation model γ_i [Eq. (1)] and the void ratio evolution model e_i [Eq. (2)] allow us to compute the incremental plastic vertical strain $\Delta\varepsilon_z^{pl}$ and plastic volumetric strain $\Delta\varepsilon_{vol}^{pl}$ between two consecutive cycles i and $i+1$. This approach avoids the inherent error magnification in incremental computations using experimental data

$$\Delta\varepsilon_z^{pl}\Big|_i = \varepsilon_z^{pl}\Big|_{i+1} - \varepsilon_z^{pl}\Big|_i \tag{6}$$

$$\Delta\varepsilon_{vol}^{pl}\Big|_i = \frac{e_{i+1} - e_i}{1 + e_i} \tag{7}$$

For small strains, the ratio ν^* between the incremental horizontal-to-vertical plastic strains in axisymmetric conditions is

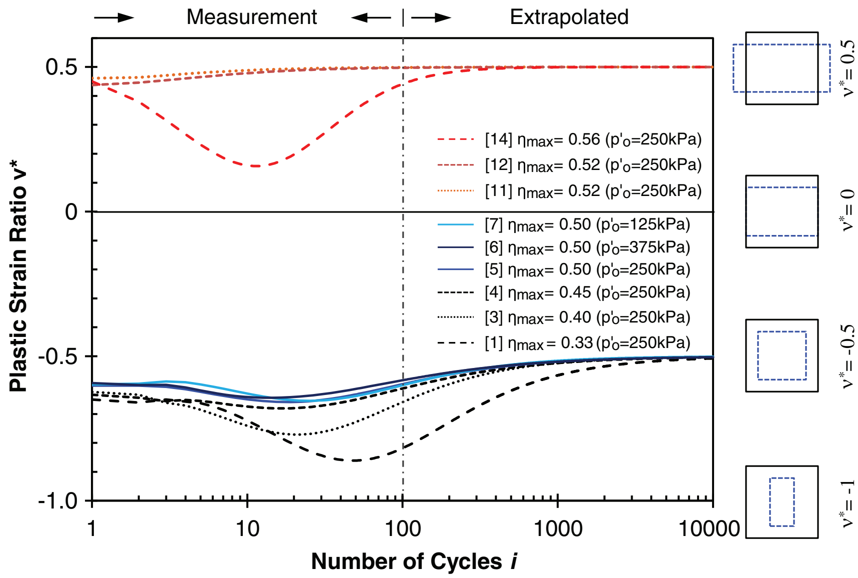

Fig. 10. (Color) Ratio between incremental horizontal-to-vertical plastic strains $\nu^* = -\Delta\varepsilon_\perp^{\text{pl}}/-\Delta\varepsilon_{//}^{\text{pl}}$ versus number of cycles. Sketches capture deformation modes. Numbers in square brackets [#] indicate the Test number in Table 2.

$$\nu^*|_i = -\frac{\Delta\varepsilon_\perp}{\Delta\varepsilon_{//}}\bigg|_{plastic} = -\frac{\frac{\Delta\varepsilon_{vol}^{pl}\big|_i - \Delta\varepsilon_z^{pl}\big|_i}{2}}{\Delta\varepsilon_z^{pl}\big|_i} = \frac{1}{2}\left(1 - \frac{\Delta\varepsilon_{vol}^{pl}\big|_i}{\Delta\varepsilon_z^{pl}\big|_i}\right) \quad (8)$$

A ratio $\nu^* = 0.5$ implies vertical deformation at constant volume (i.e., accumulation of vertical deformation at the terminal density). A ratio $\nu^* \to 0$ corresponds to volume contraction under zero-lateral strain. A negative ratio $\nu^* < 0$ indicates that both vertical and horizontal contraction take place during repetitive loading; in fact, $\nu^* = -1$ implies isotropic volume contraction. Finally, a positive ratio $\nu^* > 0$ indicates $\Delta\varepsilon_{vol}^{pl} < \Delta\varepsilon_z^{pl}$.

Fig. 10 shows the evolution of the plastic strain ratio ν^* with the number of cycles for loose, medium dense, and dense specimens. All trends exhibit an early dip into lower values of the plastic strain ratio (i.e., towards global contraction), followed by a gradual evolution to asymptotic trends.

Conclusions

Repetitive changes in pore water pressure can lead to the accumulation of plastic volumetric and shear strains. The initial state of stress and void ratio (p_o', q_o, e_o), the amplitude of pressure cycles Δu_w, and the maximum stress obliquity $\eta_{\max}$ determine the volumetric and shear strain response.

Volumetric Response

The void ratio evolves towards an asymptotic terminal void ratio e_T as the number of pressure cycles increases; the rate of change is more pronounced for high stress obliquity $\eta_{\max}$.

- The terminal void ratio for pressure cycles e_T falls below the critical state line. The void ratio at critical state e_{cs} for the same initial stress p_o' and the minimum void ratio $e_{\min}$ of the sand "bound" the terminal void ratio for pressure cycles $e_{\min} < e_T < e_{cs}$.
- The terminal void ratios for dilative and contractive specimens do not converge to a single trend.
- The terminal change in the void ratio $(e_o - e_T)$ in loose and medium dense sands increases with stress obliquity $\eta_{\max}$ and is a fraction of $(e_o - e_{\min})$; for reference, $(e_o - e_T) \leq 0.3 \cdot (e_o - e_{\min})$ in this study.
- Dense dilative sands experience minimal void ratio changes and only dilate when $\eta_{\max}$ approaches the critical state, $\eta_{\max} \geq 0.95 \cdot \eta_{cs}$. Consequently, the frictional resistance evolves from ϕ_{peak} towards ϕ_{cs} and soils may fail in shear during subsequent pressure cycles.

Shear Response

The shear strain accumulation is more pronounced in earlier cycles, in loose sands, in specimens subjected to higher initial mean stress p_o' and in specimens that experience a higher maximum stress obliquity $\eta_{\max}$.

- The shear deformation may stabilize at shakedown, or continue in ratcheting mode. The maximum stress obliquity $\eta_{\max}$ is the best predictor of shakedown or ratcheting.
- Shakedown should be expected as long as pressure amplitudes keep the stress obliquity below $\eta_{\max} < 0.95 \cdot \eta_{cs}$. Conversely, ratcheting takes place when the maximum stress obliquity approaches or exceeds $\eta_{\max} \geq 0.95 \cdot \eta_{cs}$.

Volumetric and shear strain accumulation during repetitive pressure cycles requires a minimum threshold strain which is estimated to be $\gamma \approx 5 \times 10^{-4}$ in this study. A particle-level analysis of contact loss and published experimental data show that the threshold strain increases with confinement p'.

Acknowledgments

The KAUST endowment funded this research. Gabrielle E. Abelskamp edited the manuscript.

References

Abuel-Naga, H. M., D. T. Bergado, and A. Bouazza. 2007. "Thermally induced volume change and excess pore water pressure of soft Bangkok clay." *Eng. Geol.* 89 (1–2): 144–154. https://doi.org/10.1016/j.enggeo.2006.10.002.

Albrecht, B. A., and C. H. Benson. 2001. "Effect of desiccation on compacted natural clays." *J. Geotech. Geoenviron. Eng.* 127 (1): 67–75. https://doi.org/10.1061/(ASCE)1090-0241(2001)127:1(67).

Alonso-Marroquin, F., and H. J. Herrmann. 2004. "Ratcheting of granular materials." *Phys. Rev. Lett.* 92 (5): 054301. https://doi.org/10.1103/PhysRevLett.92.054301.

Anderson, S. A., and N. Sitar. 1995. "Analysis of rainfall-induced debris flows." *J. Geotech. Eng.* 121 (7): 544–552. https://doi.org/10.1061/(ASCE)0733-9410(1995)121:7(544).

Brenner, R. P. 1985. "Field stress path simulation of rain-induced slope failure." In Vol. 2 of *Proc. 11th ICSMFE*, 991–996. Rotterdam, Netherlands: A.A. Balkema.

Cai, Y., T. Wu, L. Guo, and J. Wang. 2018. "Stiffness degradation and plastic strain accumulation of clay under cyclic load with principal stress rotation and deviatoric stress variation." *J. Geotech. Geoenviron. Eng.* 144 (5): 04018021. https://doi.org/10.1061/(ASCE)GT.1943-5606.0001854.

Castro G., S. J. Poulos, J. W. France, and J. L. Enos. 1982. *Liquefaction induced by cyclic loading*. NASA STI/Recon Technical Report N, 83. Winchester, MA: Geotechnical Engineers Inc.

Chamberlain, E. J., I. Iskandar, and S. E. Hunsicker. 1990. "Effect of freeze-thaw cycles on the permeability and macrostructure of soils." *Cold Region Res. Eng. Lab.* 90 (1): 145–155.

Chang, W. J., S. H. Shou, and A. B. Huang. 2017. "Mechanism of subsidence from pore pressure fluctuation in aquifer layers." In *Proc. 19th Int. Conf. Soil Mechanics and Geotechnical Engineering*. Seoul: International Society for Soil Mechanics and Geotechnical Engineering.

Chod , G. C., J. Dodds, and J. C. Santamarina. 2006. "Particle shape effects on packing density, stiffness, and strength: Natural and crushed sands." *J. Geotech. Geoenviron. Eng.* 132 (5): 591–602. https://doi.org/10.1061/(ASCE)1090-0241(2006)132:5(591).

Chong, S. H., and J. C. Santamarina. 2016. "Sands subjected to vertical repetitive loading under zero lateral strain: Accumulation models, terminal densities, and settlement." *Can. Geotech. J.* 53 (12): 2039–2046. https://doi.org/10.1139/cgj-2016-0032.

Chu, J., S. Leroueil, and W. K. Leong. 2003. "Unstable behaviour of sand and its implication for slope instability." *Can. Geotech. J.* 40 (5): 873–885. https://doi.org/10.1139/t03-039.

Croney, D., and J. D. Coleman. 1954. "Soil structure in relation to soil suction (pF)." *Eur. J. Soil Sci.* 5 (1): 75–84. https://doi.org/10.1111/j.1365-2389.1954.tb02177.x.

da Fonseca, A. V., S. Rios, M. F. Amaral, and F. Panico. 2013. "Fatigue cyclic tests on artificially cemented soil." *Geotech. Test. J.* 36 (2): 227–235. https://doi.org/10.1520/GTJ20120113.

Díaz-Rodríguez, J. A., and J. C. Santamarina. 2001. "Mexico City soil behavior at different strains: Observations and physical interpretation." *J. Geotech. Geoenviron. Eng.* 127 (9): 783–789. https://doi.org/10.1061/(ASCE)1090-0241(2001)127:9(783).

Dobry, R., R. S. Ladd, F. Y. Yokel, R. M. Chung, and D. Powell. 1982. "Prediction of pore water pressure buildup and liquefaction of sands during earthquakes by the cyclic strain method." In *Building science series 138*. Washington, DC: US Department of Commerce, National Bureau of Standards.

Dyvik, R., R. Dobry, G. E. Thomas, and W. G. Pierce. 1984. *Influence of consolidation shear stresses and relative density on threshold strain and pore pressure during cyclic straining of saturated sand*. Miscellaneous Paper GL-84-15. Washington, DC: Dept. of the Army, USACE.

Farooq, K., R. Orense, and I. Towhata. 2004. "Response of unsaturated sandy soils under constant shear stress drained condition." *Soils. Found.* 44 (2): 1–13. https://doi.org/10.3208/sandf.44.2_1.

Gambolati, G., and P. Teatini. 2015. "Geomechanics of subsurface water withdrawal and injection." *Water Resour. Res.* 51 (6): 3922–3955. https://doi.org/10.1002/2014WR016841.

Gu, C., Z. Gu, Y. Cai, J. Wang, and Q. Dong. 2018. "Effects of cyclic intermediate principal stress on the deformation of saturated clay." *J. Geotech. Geoenviron. Eng.* 144 (8): 04018052. https://doi.org/10.1061/(ASCE)GT.1943-5606.0001924.

Huang, A. W. 2016. "The seventh James. K. Mitchell lecture: Characterization of silty/sand soils." *Aust. Geomech. J.* 51 (4): 1–23.

Hung, W. C., C. Hwang, J. C. Liou, Y. S. Lin, and H. L. Yang. 2012. "Modeling aquifer-system compaction and predicting land subsidence in central Taiwan." *Eng. Geol.* 147–148 (Oct): 78–90. https://doi.org/10.1016/j.enggeo.2012.07.018.

Ishihara, K. 1996. *Soil behaviour in earthquake geotechnics*. Oxford, New York: Clarendon Press; Oxford University Press.

Johnson, K. L. 1986. "Plastic flow, residual stress and shakedown in rolling contact." In *Proc. 2nd Int. Conf. on Contact Mechanics and Wear of Rail/Wheel Systems.* Waterloo, ON: Univ. of Rhode Island.

Kim, D. S. 1991. "Deformational characteristics of soils at small to intermediate strains from cyclic test." Ph.D. thesis, Dept. of Civil Architectural and Environmental Engineering, Univ. of Texas.

Laloui, L. 2001. "Thermo-mechanical behaviour of soils." *Rev. Française Génie Civ.* 5 (6): 809–843. https://doi.org/10.1080/12795119.2001.9692328.

Leroueil, S., J. Chu, and D. Wanatowski. 2009. "Slope instability due to pore water pressure increase." In *Proc., 1st Italian Workshop on Landslides*, 8–10. Naples, Italy: Doppiavoce.

Mohamad, R., and R. Dobry. 1986. "Undrained monotonic and cyclic triaxial strength of sand." *J. Geotech. Eng.* 112 (10): 941–958. https://doi.org/10.1061/(ASCE)0733-9410(1986)112:10(941).

Mueth, D. M., G. F. Debregeas, G. S. Karczmart, P. J. Eng, S. R. Nagel, and H. M. Jaeger. 2000. "Signatures of granular microstructure in dense shear flows." *Nature* 406 (6794): 385–389. https://doi.org/10.1038/35019032.

Musso, G., E. R. Morales, A. Gens, and E. Castellanos. 2003. "The role of structure in the chemically induced deformations of FEBEX bentonite." *Appl. Clay Sci.* 23 (1–4): 229–237. https://doi.org/10.1016/S0169-1317(03)00107-8.

Nakata, Y., T. Kajiwara, and N. Yoshimoto. 2013. "Collapse behavior of slope due to change in pore water pressure." In *Proc., 18th Int. Conf. Soil Mechanics and Geotechnical Engineering*, 2225–2228. Paris: International Society for Soil Mechanics and Geotechnical Engineering.

Narsilio, A., and J. C. Santamarina. 2008. "Terminal densities." *Géotechnique* 58 (8): 669–674.

Ohtsuka, S. 2007. "Shear behavior of clay in slope for pore water pressure increase." In *Progress in landslide science*, 295–303. Berlin: Springer.

Ohtsuka, S., and Y. Miyata. 2001. "Consideration on landslide mechanism based on pore water pressure loading test." In Vol. 2 of *Proc., Int. Conf. Soil Mechanics and Geotechnical Engineering*, 1233–1236. London: International Society for Soil Mechanics and Geotechnical Engineering.

Olson, S. M., T. D. Stark, W. H. Walton, and G. Castro. 2000. "1907 static liquefaction flow failure of the north dike of Wachusett dam." *J. Geotech. Geoenviron. Eng.* 126 (12): 1184–1193. https://doi.org/10.1061/(ASCE)1090-0241(2000)126:12(1184).

Ono, T., and T. Mitachi. 1997. "Computer controlled triaxial freeze-thaw-shear apparatus." In *Ground freezing*, 335–339. Rotterdam: A. A. Balkema.

O'Reilly, M. P., and S. F. Brown. 1991. *Cyclic loading of soils: From theory to design*. Glasgow, UK: Blackie.

Orense, R., K. Farooq, and I. Towhata. 2004. "Deformation behavior of sandy slopes during rainwater infiltration." *Soils. Found.* 44 (2): 15–30. https://doi.org/10.3208/sandf.44.2_15.

Page, D., P. Dillon, J. Vanderzalm, S. Toze, J. Sidhu, K. Barry, K. Levett, S. Kremer, and R. Regel. 2010. "Risk assessment of aquifer storage transfer and recovery with urban stormwater for producing water of a potable quality." *J. Environ. Qual.* 39 (6): 2029–2039. https://doi.org/10.2134/jeq2010.0078.

Park, J., and J. C. Santamarina. 2019. "Sand response to a large number of loading cycles under zero-lateral strain conditions: Evolution of void ratio and small strain stiffness." *Géotechniqué* 69 (6): 501–513. https://doi.org/10.1680/jgeot.17.P.124.

Premchitt, J., E. W. Brand, and H. B. Phillipson. 1986. "Landslides caused by rapid groundwater changes." *Geol. Soc. London, Eng. Geol. Spec. Publ.* 3 (1): 87–94. https://doi.org/10.1144/GSL.ENG.1986.002.01.09.

Qi, J., P. A. Vermeer, and G. Cheng. 2006. "A review of the influence of freeze-thaw cycles on soil geotechnical properties." *Permafrost*

Periglacial Processes 17 (3): 245–252. https://doi.org/10.1002/ppp.559.

Santamarina, J. C., and G. C. Cho. 2001. “Determination of critical state parameters in sandy soils-simple procedure.” *Geotech. Test. J.* 24 (2): 185–192. https://doi.org/10.1520/GTJ11338J.

Santamarina, J. C., K. A. Klein, and M. A. Fam. 2001. *Soils and waves: Particulate materials behavior, characterization and process monitoring*. Chichester, UK: Wiley.

Santamarina, J. C., and H. Shin. 2009. “Friction in granular media.” In *Meso-scale shear physics in earthquake and landslide mechanics*, 157–188. London: CRC Press.

Schofield, A. N., and P. Wroth. 1968. *Critical state soil mechanics*. London: McGraw-Hill.

Sharp, R. W., and J. R. Booker. 1984. “Shakedown of pavements under moving surface loads.” *J. Transp. Eng.* 110 (1): 1–14. https://doi.org/10.1061/(ASCE)0733-947X(1984)110:1(1).

Shi, X., S. Jiang, H. Xu, F. Jiang, Z. He, and J. Wu. 2016. “The effects of artificial recharge of groundwater on controlling land subsidence and its influence on groundwater quality and aquifer energy storage in Shanghai, China.” *Environ. Earth. Sci.* 75 (3): 195. https://doi.org/10.1007/s12665-015-5019-x.

Silver, M. L., and H. B. Seed. 1971. “Volume changes in sands during cyclic loading.” *J. Soil Mech. Found. Div.* 97 (9): 1171–1182.

Skempton, A. W. 1961. “Effective stress in soils, concrete and rocks.” In *Proc., Pore Pressure and Suction in Soils Conf.* 4–16. London: Butterworths.

Taylor, D. W. 1948. *Fundamentals of soil mechanics*. New York: Wiley.

Triantafyllidis, T., T. Wichtmann, and A. Niemunis. 2004. “On the determination of cyclic strain history.” In *Proc., CBS04*, 321–332. Rotterdam, Netherlands: A.A. Balkema.

Viklander, P. 1998. “Permeability and volume changes in till due to cyclic freeze/thaw.” *Can. Geotech. J.* 35 (3): 471–477. https://doi.org/10.1139/t98-015.

Vucetic, M. 1994. “Cyclic threshold shear strains in soils.” *J. Geotech. Geoenviron. Eng.* 120 (12): 2208–2228. https://doi.org/10.1061/(ASCE)0733-9410(1994)120:12(2208).

Werkmeister, S. 2003. “Permanent deformation behaviour of unbound granular materials in pavement constructions.” Ph.D. thesis, Fakultät Bauingenieurwesen, Technischen Universität.

Werkmeister, S., A. R. Dawson, and F. Wellner. 2005. “Permanent deformation behaviour of granular materials.” *Road. Mater. Pavement.* 6 (1): 31–51. https://doi.org/10.1080/14680629.2005.9689998.

Wichtmann, T., A. Niemunis, and T. Triantafyllidis. 2005. “Strain accumulation in sand due to cyclic loading: Drained triaxial tests.” *Soil Dyn. Earthquake Eng.* 25 (12): 967–979. https://doi.org/10.1016/j.soildyn.2005.02.022.

Wu, T., Y. Cai, L. Guo, D. Ling, and J. Wang. 2017. “Influence of shear stress level on cyclic deformation behaviour of intact Wenzhou soft clay under traffic loading.” *Eng. Geol.* 228 (Oct): 61–70. https://doi.org/10.1016/j.enggeo.2017.06.013.

Youd, T. L. 1973. “Factors controlling maximum and minimum densities of sands.” In *Evaluation of relative density and its role in geotechnical projects involving cohesionless soils*, edited by E. Selig, and R. Ladd. 98–112. West Conshohocken, PA: ASTM.